Use of Density Functional Based Tight Binding Methods in Vibrational Circular Dichroism

Teodoro, T. Q.; Koenis, M. A.J.; Rüger, R.; Galembeck, S. E.; Buma, W. J.; Nicu, V. P.; Visscher, L.

published in
Journal of Physical Chemistry A
2018

DOI (link to publisher)
10.1021/acs.jpca.8b08218

document version
Publisher's PDF, also known as Version of record

THE JOURNAL OF PHYSICAL CHEMISTRY A

Article

Cite This: J. Phys. Chem. A 2018, 122, 9435−9445

pubs.acs.org/JPCA

Use of Density Functional Based Tight Binding Methods in Vibrational Circular Dichroism

T. Q. Teodoro,[†,‡] M. A. J. Koenis,[§] R. Rüger,[∥] S. E. Galembeck,[†] W. J. Buma,[§] V. P. Nicu,[⊥] and L. Visscher*[,‡]

[†]Departamento de Química, FFCLRP, Universidade de São Paulo, Avenida Bandeirantes 3900, Ribeirão Preto, 14040-901 São Paulo Brazil

[‡]Amsterdam Center for Multiscale Modeling, Faculty of Science, Vrije Universiteit Amsterdam, de Boelelaan 1083, 1081 HV Amsterdam, The Netherlands

[§]Van't Hoff Institute for Molecular Sciences, University of Amsterdam, Science Park 904, 1098 XH Amsterdam, The Netherlands

[∥]Software for Chemistry & Materials BV, De Boelelaan 1083, 1081 HV Amsterdam, The Netherlands

[⊥]Department of Environmental Science, Physics, Physical Education and Sport, Lucian Blaga University of Sibiu, loan Ratiu Street, Nr. 7-9, 550012 Sibiu, Romania

Supporting Information

ABSTRACT: Vibrational circular dichroism (VCD) is a spectroscopic technique used to resolve the absolute configuration of chiral systems. Obtaining a theoretical VCD spectrum requires computing atomic polar and axial tensors on top of the computationally demanding construction of the force constant matrix. In this study we evaluated a VCD model in which all necessary quantities are obtained with density functional based tight binding (DFTB) theory. The analyzed DFTB parametrizations fail at providing accurate vibrational frequencies and electric dipole gradients but yield reasonable normal modes at a fraction of the computational cost of density functional theory (DFT). Thus, by applying DFTB in composite methods along with DFT, we show that it is possible to obtain accurate VCD spectra at a much lower computational demand.

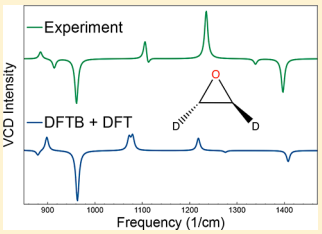

INTRODUCTION

Chiral molecules are defined as systems for which the mirror images (enantiomers) of the same isomer are nonsuperimposable on each other. These enantiomers interact differently with other chiral systems, which have important consequences, for example, for their biological functioning. Resolving the absolute configuration of chiral molecules is therefore of fundamental importance for chemistry and biological sciences. Vibrational circular dichroism (VCD)[1,2] is one of the most powerful spectroscopic techniques for investigating molecular chirality under conditions in which the molecule of interest is actually employed. This tool uses the difference in absorption of left and right circularly polarized light in the infrared region of the electromagnetic spectrum (see refs 3−8 for reviews on VCD and other vibrational optical properties). The experimental VCD spectrum is then assigned to one particular enantiomer by comparison with theoretical calculations.

Currently, most VCD implementations in standard quantum chemistry packages rely on Stephens equations,[9] which require calculating electric and magnetic perturbations in addition to the computationally demanding solution of $3N_{atoms}$ response equations to obtain derivatives of the molecular electronic wave function with respect to nuclear displacements. This poses a challenge as the computational cost increases rapidly with molecular size. In addition, VCD spectra are highly sensitive to conformational changes,[10] which adds another dimension to the set of calculations that needs to be performed for a thorough analysis. Even studies carried out with fairly efficient density functional theory (DFT) methods may therefore already become infeasible for molecules with a few hundred atoms, unless large computational resources can be allocated. This is unfortunate as the VCD technique is particularly of interest when studying large organic molecules, e.g., peptides and pharmaceutical agents.[11] This raises the interest in lower, yet sufficient reliable, levels of theory that may tackle such systems in a routine fashion.

Looking at methods with smaller computational demands than DFT, one may consider the density functional based tight binding (DFTB) method, which is based on an expansion of the Kohn−Sham total energy in DFT with respect to charge fluctuations.[12,13] This ansatz, which is combined with several other approximations, such as the use of a minimal basis, yields calculations that are a couple of orders of magnitude faster than standard DFT ones. A fair amount of literature can be found about the reliability of DFTB for predicting fundamental properties, such as molecular geometry and vibrational frequencies (see, e.g., refs 14−18). Studies on more intricate properties are however still scarce, even though promising

Received: August 23, 2018
Revised: November 9, 2018
Published: November 19, 2018

DOI: 10.1021/acs.jpca.8b08218
J. Phys. Chem. A 2018, 122, 9435−9445

results have been obtained for, e.g., first hyperpolarizabilities.[19,20] In the works of Jalkanen and co-workers,[21,22] DFTB was also successfully applied in composite methods to yield VCD and vibrational absorption (VA) spectra for *N*-acetyl-L-alanine-*N*′-methyl amide and propylene oxide. Those results showed some agreement with experimental spectra, but to the best of our knowledge, no implementation has been done in which VCD could be fully calculated within a DFTB framework. Neither has a systematic analysis on several DFTB methods to evaluate their advantages/disadvantages for VCD been carried out. In the present study we use the tools available in the DFTB engine[23] of the Amsterdam Density Functional modeling suite (ADF)[24,25] to fully assess the performance of standard DFTB parametrizations in an implementation of a DFTB-based VCD model.

THEORY

The dipole strength $\mathcal{D}_n^{|\nu\rangle\rightarrow|\nu'\rangle}$ for the transition $|\nu\rangle \rightarrow |\nu'\rangle$ of the nth vibrational mode (which yields the VA intensity of the mode) is given by the squared modulus of the electric transition dipole moment operator:

$$\mathcal{D}_n^{|\nu\rangle\rightarrow|\nu'\rangle} = [\langle\nu|\hat{\mu}_e|\nu'\rangle_n]^2 \tag{1}$$

For circular dichroism, the intensity associated with the transition between these same vibrational states is proportional to the rotational strength $\mathcal{R}_n^{|\nu\rangle\rightarrow|\nu'\rangle}$, which is defined as the imaginary part of the dot product between the electric and magnetic transition dipole moment operators:

$$\mathcal{R}_n^{|\nu\rangle\rightarrow|\nu'\rangle} = \Im[\langle\nu|\hat{\mu}_e|\nu'\rangle_n \cdot \langle\nu'|\hat{\mu}_m|\nu\rangle_n] \tag{2}$$

Considering the fundamental transition $|0\rangle \rightarrow |1\rangle$ and using standard assumptions, such as the absence of anharmonicity, each i component of the dipole transition moments can be expressed in terms of atomic contributions as[9]

$$\langle 0|(\hat{\mu}_e)_i|1\rangle_n = \left(\frac{\hbar}{2\omega_n}\right)^{1/2} \sum_{\mathcal{A}} \sum_{\alpha} P^i_{\mathcal{A},\alpha} S^n_{\mathcal{A},\alpha} \tag{3}$$

and

$$\langle 0|(\hat{\mu}_m)_i|1\rangle_n = -(2\hbar^3\omega_n)^{1/2} \sum_{\mathcal{A}} \sum_{\alpha} A^i_{\mathcal{A},\alpha} S^n_{\mathcal{A},\alpha} \tag{4}$$

where α are Cartesian components of atomic displacements, $\mathcal{A}$ runs over all the nuclei in the molecule, $\hbar$ is the reduced Planck constant, ω_n is the harmonic angular frequency of the nth normal mode, and the summands are defined as follows:

- $S^n_{\mathcal{A},\alpha}$ are the elements of the transformation matrix that relates Cartesian displacements to the mass-weighted normal mode displacements ($\vec{Q}^n$):

$$R_{\mathcal{A},\alpha} - R^0_{\mathcal{A},\alpha} = \sum_n S^n_{\mathcal{A},\alpha} Q^n_{\mathcal{A},\alpha} \tag{5}$$

in which $R^0_{\mathcal{A},\alpha}$ and $R_{\mathcal{A},\alpha}$ are, respectively, the equilibrium and displaced α coordinates of the $\mathcal{A}$ atoms.

- $P^i_{\mathcal{A},\alpha}$ represent the elements of the geometry-derivative tensor of the electric dipole moment in the ground state, commonly known as the atomic polar tensor (APT):[26]

$$P^i_{\mathcal{A},\alpha} = \left[\frac{\partial(\vec{\mu}_e)_i}{\partial R_{\mathcal{A},\alpha}}\right]_0 \tag{6}$$

- $A^i_{\mathcal{A},\alpha}$ define the elements of the tensor of the derivatives of the ground state magnetic moment with respect to the velocity of the nuclei, also known as the atomic axial tensor (AAT):

$$A^i_{\mathcal{A},\alpha} = \left[\frac{\partial(\vec{\mu}_m)_i}{\partial \dot{R}_{\mathcal{A},\alpha}}\right]_0 \tag{7}$$

Calculating the components of the transformation matrix $\mathbf{S}^n$ (eq 5) is by far the most computationally demanding step for obtaining VA and VCD spectra, as this requires solving $3N_{atoms}$ response equations to construct the Hessian (the force constant matrix). Implementations of a VCD code in DFT packages, like the one available in ADF,[27] make it feasible to treat molecules containing a few dozen or even a couple of hundred atoms. With the need to sample many conformations as well, the total calculation time may still become prohibitive for routine use, however. As a faster alternative, we will therefore consider DFTB, which describes the Kohn−Sham energy in terms of a precalculated reference density and a perturbation. By expanding the exchange−correlation energy as a Taylor series, the range of the expansion that is taken into account defines the DFTB model (a good review on the topic can be found in ref 28).

In the original DFTB model (hereafter denoted DFTB1),[13] the energy is calculated as

$$E^{\mathrm{DFTB1}} = \sum_{o}^{N_{occ}} \sum_{\mu}^{N_{bas}} \sum_{\nu}^{N_{bas}} c_{\mu o} c_{\nu o} H^0_{\mu\nu} + \frac{1}{2} \sum_{\mathcal{AB}} V^{rep}_{\mathcal{AB}} \tag{8}$$

in which $H^0_{\mu\nu}$ is the effective Kohn−Sham Hamiltonian, $V^{rep}_{\mathcal{AB}}$ is the repulsive potential, and $c_{\mu o}$ are expansion coefficients of molecular orbitals ϕ_o in a (usually) minimal basis of atomic valence orbitals χ:

$$\phi_o = \sum_{\mathcal{A}} \sum_{\mu\in\mathcal{A}} c_{\mu o} \chi_\mu \tag{9}$$

The Hamiltonian and the overlap matrix ($S_{\mu\nu} = \langle\chi_\mu|\chi_\nu\rangle$) elements are precalculated and tabulated using the Slater−Koster technique,[29] so the respective terms do not have to be computed on the fly during the calculation. With this efficient interpolation technique the cost of constructing the Hamiltonian is greatly reduced and the bottleneck is typically only the diagonalization of the Hamiltonian. At some extra expense, results can generally be improved by using second- and third-order terms of the Taylor series in the self-consistent-charge models (SCC-DFTB) DFTB2[30] and DFTB3,[31] respectively.

The DFTB1, DFTB2, and DFTB3 models are all available in the ADF modeling suite.[23,25] In the 2017 version of the latter package, the DFTB calculations of the force constant matrix were done numerically in a two-sided evaluation of the analytical gradients of the energy at distorted geometries. By using Mulliken population analysis,[32] the atomic partial charges, $q_{\mathcal{A}}$, yield electric dipole moments

$$\vec{\mu}_e \approx \sum_{\mathcal{A}} q_{\mathcal{A}} \vec{R}_{\mathcal{A}} \tag{10}$$

at each of these displaced geometries, giving the APT tensor with virtually no extra computational cost:

DOI: 10.1021/acs.jpca.8b08218
J. Phys. Chem. A 2018, 122, 9435−9445

$$P^{i}_{\mathcal{A},\alpha} \approx \frac{(\vec{\mu}_e)_i|_{\mathbf{R}^0+0.5d_{\mathcal{A},\alpha}} - (\vec{\mu}_e)_i|_{\mathbf{R}^0-0.5d_{\mathcal{A},\alpha}}}{d_{\mathcal{A},\alpha}} \tag{11}$$

where $d_{\mathcal{A},\alpha} = R_{\mathcal{A},\alpha} - R^0_{\mathcal{A},\alpha}$ is the size of the nuclear ($\mathcal{A}$) displacement in the α direction. The calculation of dipole strengths (eq 1) was thus already possible with the DFTB engine of ADF and VA intensities are straightforwardly obtained.

The only missing ingredient needed to obtain VCD intensities is therefore the AAT tensor defined in eq 7. A straightforward evaluation would require performing magnetic response calculations which would be considerably more involved than the electric ones. With the DFTB method, it is, however, also appropriate to consider a simpler approximation to the magnetic tensor. In the so-called atomic polar tensor (APT) model,[33] introduced by Freedman and Nafie, the magnetic term assumes a form that depends on the electric dipole gradients. In this formalism, the rotational strength is approximated as

$$\mathcal{R}_n^{|0\rangle\rightarrow|1\rangle}(\mathrm{APT}) = \frac{\hbar}{4c}\sum_i \left\{\left[\sum_{\mathcal{A}} \vec{P}^{\,i}_{\mathcal{A}}\cdot\vec{S}^{\,n}_{\mathcal{A}}\right]\left[\sum_{\mathcal{A}} \vec{T}^{\,i}_{\mathcal{A}}\cdot\vec{S}^{\,n}_{\mathcal{A}}\right]\right\} \tag{12}$$

where the $\vec{T}^{\,i}_{\mathcal{A}}$ vectors are rows in the $\mathbf{T}_{\mathcal{A}}$ matrix, whose columns are given by

$$\vec{T}_{\mathcal{A},\alpha} = \vec{R}^{\,0}_{\mathcal{A}} \times \left(\frac{\partial\vec{\mu}_e}{\partial R_{\mathcal{A},\alpha}}\right) \tag{13}$$

This approximation makes it possible to compute VCD spectra fully within a DFTB framework with no additional implementation besides adding together already available components in accordance with eq 12. This yields a fast and simple tool that can be easily used for analysis before considering more elaborate schemes such as Stephens equations.[9] We note in passing that eq 13 leads to origin-independent rotational strengths as the following condition is always satisfied:[34]

$$(T^i_{\mathcal{A},\alpha})^{\vec{O}_1} = (T^i_{\mathcal{A},\alpha})^{\vec{O}_2} + \sum_{\gamma\delta}\epsilon_{i\gamma\delta}Y_\gamma P^{\delta}_{\mathcal{A},\alpha} \tag{14}$$

in which $\vec{Y} = \vec{O}_2 - \vec{O}_1$ is the displacement vector between two origins and ϵ is the Levi-Civita tensor.

COMPUTATIONAL DETAILS

DFT calculations were carried out using the 2017 version of the ADF modeling suite,[24,25] with the Becke–Perdew exchange–correlation potential (BP86),[35−37] a generalized gradient approximation (GGA) functional, in combination with Slater type orbital (STO) nonrelativistic valence triple-ζ basis sets extended with one polarization function (TZP).[38] All electrons were treated explicitly (no frozen core). The VCD calculations at this DFT level were done by means of the Nicu et al.[27] implementation of Stephens equations (hence both APT and AAT tensors are calculated). Regarding the DFTB calculations, the respective engine within ADF was modified to include the implementation of eq 12 (where only the APTs are needed). Besides the classic tight-binding model Hamiltonian without self-consistency cycles (DFTB1),[13] self-consistent-charges (DFTB2)[30] and third-order expansion (DFTB3)[31] calculations were carried out as well. The DFTB parameters used throughout this study were taken from the Slater–Koster files for organic molecules and biomolecules, mio-1-1 (proper for DFTB2),[30] 3ob-3-1 (designed for DFTB3), and 3ob-freq-1-2 (a modified 3ob version intended for a better description of vibrational frequencies),[39] and QUASINANO2015.[40] For all nonmentioned criteria, default values (as in the release ADF 2017 version) were applied in all calculations. All spectra displayed in the following were broadened using a Lorentzian band shape with a half-width at half-maximum of 4 cm^{-1}.

RESULTS AND DISCUSSION

The structures of the three molecules considered in this section are depicted in Figure 1. The first two molecules are

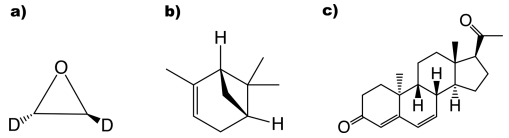

Figure 1. Structures of (a) oxirane, (b) α-pinene, and (c) dydrogesterone.

standard systems in VCD evaluations: (*S*,*S*)-[2,3-$^2H_2$]oxirane and (+)-α-pinene. Due to their rigid structure only one conformation is populated. Additionally, the simple spectra with only a handful of bands in both cases are easier to evaluate at this stage. To further validate the analysis, we also consider a larger system, a pharmaceutical compound, dydrogesterone.

Oxirane. Figures 2 (VA) and 3 (VCD) show the comparison between calculated and experimental[41] vibrational spectra (Table S1 displays the raw data, i.e., vibrational frequencies, dipole strengths, and rotational strengths). Due to the limited number of bands, peaks can be easily assigned making the comparison between theory and experiment unambiguous. As expected, the BP86/TZP calculation (when applying Stephens equations) reproduces the experimental VA and VCD spectra very well, which confirms that the results at this level of theory can be taken as the reference for the comparison with the lower level (DFTB) calculations. Regarding the spectra obtained by the several DFTB variants, one finds little correlation between any of those and the respective BP86/TZP results (mean absolute errors are considerably high irrespective of the DFTB variation). By only evaluating the VCD spectra, one could attribute such discrepancies to the APT model. The BP86/TZP calculation carried out with the APT model yields several bands with different signs than those predicted with Stephens equations. The unreliability of the APT model for predicting VCD bands has been previously reported,[42,43] and its implementation should not be blindly applied beyond a quick assessment. However, even when comparing the DFTB results with the BP86/TZP data from the APT model, one still finds virtually no correlation between the two levels. Additionally, there is no similar model approximation in the VA results with DFTB, and those also differ significantly from the BP86/TZP figures. It is also noticeable that the SCC-DFTB calculations with mio and 3ob parameters yield very similar spectra, which indicates the occurrence of systematic deviations in comparison with the BP86/TZP results. Thus, in order to identify the source of these deviations, and, more generally, the reasons why these standard DFTB parametrizations fail at even providing

DOI: 10.1021/acs.jpca.8b08218
J. Phys. Chem. A 2018, 122, 9435−9445

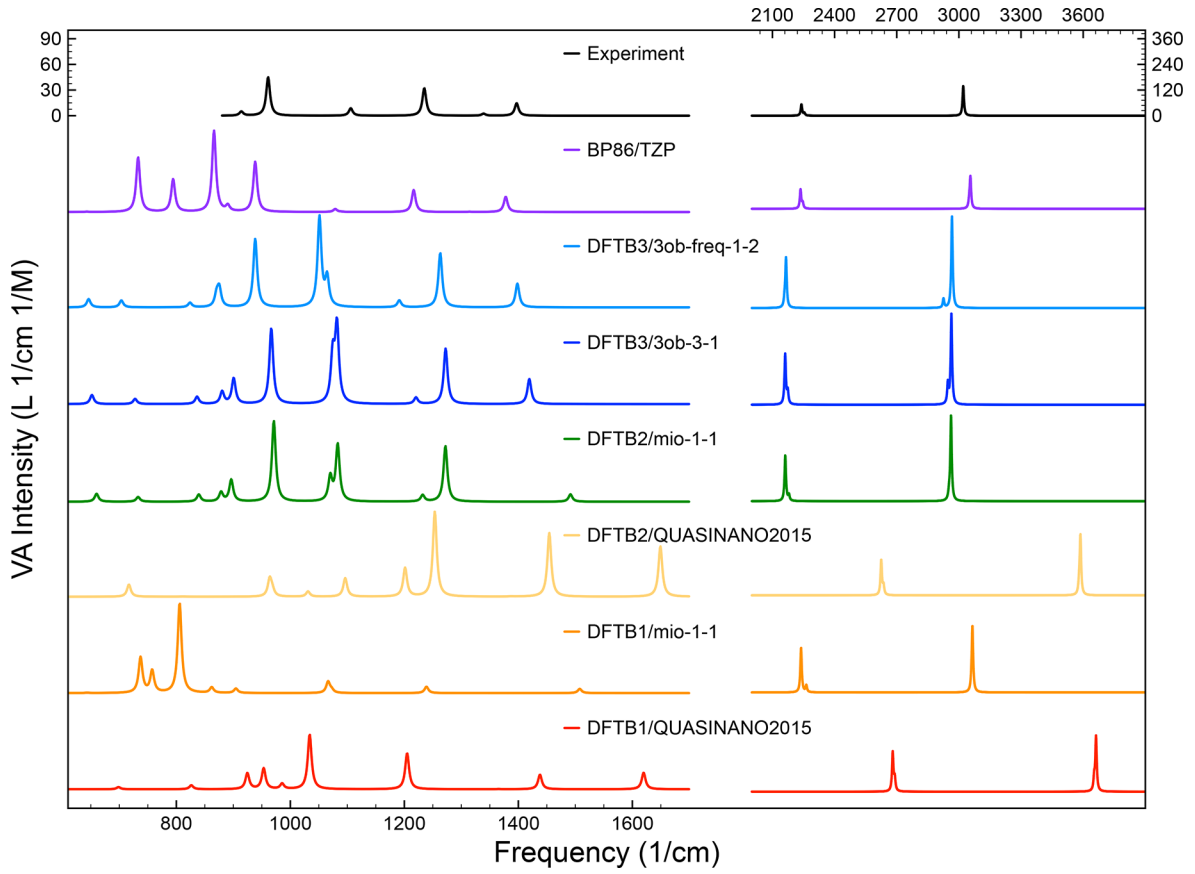

Figure 2. Comparison of VA spectra of (*S*,*S*)-[2,3-$^2H_2$]oxirane (gas phase) calculated at several levels, and experimental data from ref 41. DFTB2/QUASINANO2015, DFTB1/mio-1-1, and DFTB1/QUASINANO2015 intensities in the frequency range below 2000 cm^{-1} were rescaled by factors of, respectively, 0.6, 0.1, and 0.1 for better visualization. Bands above 2000 cm^{-1} are displayed on a different scale (shown to the right and on the top) than those in the fingerprint region. Frequencies and dipole strengths are given in Table S1.

accurate VA spectra for oxirane, we will investigate in the following the effect of using different levels of theory for the nuclear displacement vectors, vibrational frequencies, and electric dipole gradients.

Nuclear Displacement Vectors. We start the analysis for the nuclear displacement vectors by studying how the DFTB (mass-weighted) normal modes resemble the DFT ones, i.e., by calculating the scalar product between these modes. The highest overlap between a DFTB normal mode with each respective *n*th BP86/TZP mode is shown in Table 1. The square roots of these numbers can be taken as indicative of the similarity between the modes, with values close to 1 indicating that modes are alike. This analysis shows the consistency of the normal modes computed using the various DFTB variants. For example, high frequency modes, $\nu > 2000$ cm^{-1}, are similarly represented irrespective of the level of theory that is applied (most overlaps are equal to 1.00 with an average overlap of 0.99 for these modes). This feature may be expected as standard DFTB parametrization procedures are usually carried out on the basis of training sets composed of simple molecules, such as homonuclear diatomics, H_2O, CH_4, NH_3, etc., and stretching frequencies are even used for the fitting of some parametrizations.[39] Thus, simple C−H(D) stretches should be well represented by these parametrizations.

Normal modes in the fingerprint region, however, can be much more intricate. Two examples of such modes (n = 10 and n = 11) are depicted in Figure 4. Mode 10 (Figure 4a,b), which is almost purely composed of H−C−D bending vibrations, is virtually the same whether it is calculated by DFTB3/3ob-freq-1-2 or BP86/TZP. On the other hand, mode 11 (Figure 4c,d), which mixes H−C−D bending vibrations with changes in the internal angles of the oxirane ring, have different magnitudes for the norms of the carbon displacement vectors depending on the level of theory. This shows that mode mixing is an important aspect to consider. To further investigate this mode mixing, overlaps of the reference modes with the ones calculated with the same DFT functional but a smaller set, single-ζ, are shown as well in Table 1. It is noticeable that the lowest overlap values (and lowest averages) are found in the region from ∼800 to ∼1100 cm^{-1}, which contains about a third of the calculated normal modes although it represents only about 12% of the x-axis of these vibrational spectra (considering the energy difference between modes 1 and 15). Since mode mixing is strongly dependent on the energies of the vibrational levels, slight changes in energy could lead to considerably different modes. Moreover, as it is shown in ref 44, even small changes in the nuclear displacement vectors involving polar bonds may have a dramatic impact on the VCD intensity of the respective mode. In order to quantify the effects induced in the dipole and rotational strengths by these differences in the modes, the DFTB eigenvectors were combined with the APTs and AATs from the BP86/TZP calculation, thereby eliminating the DFTB error in the tensors. Results of these composite methods are shown in Table S2.

In the limit of DFTB and DFT normal modes being identical, the dipole and rotational strengths would obviously

DOI: 10.1021/acs.jpca.8b08218
J. Phys. Chem. A 2018, 122, 9435−9445

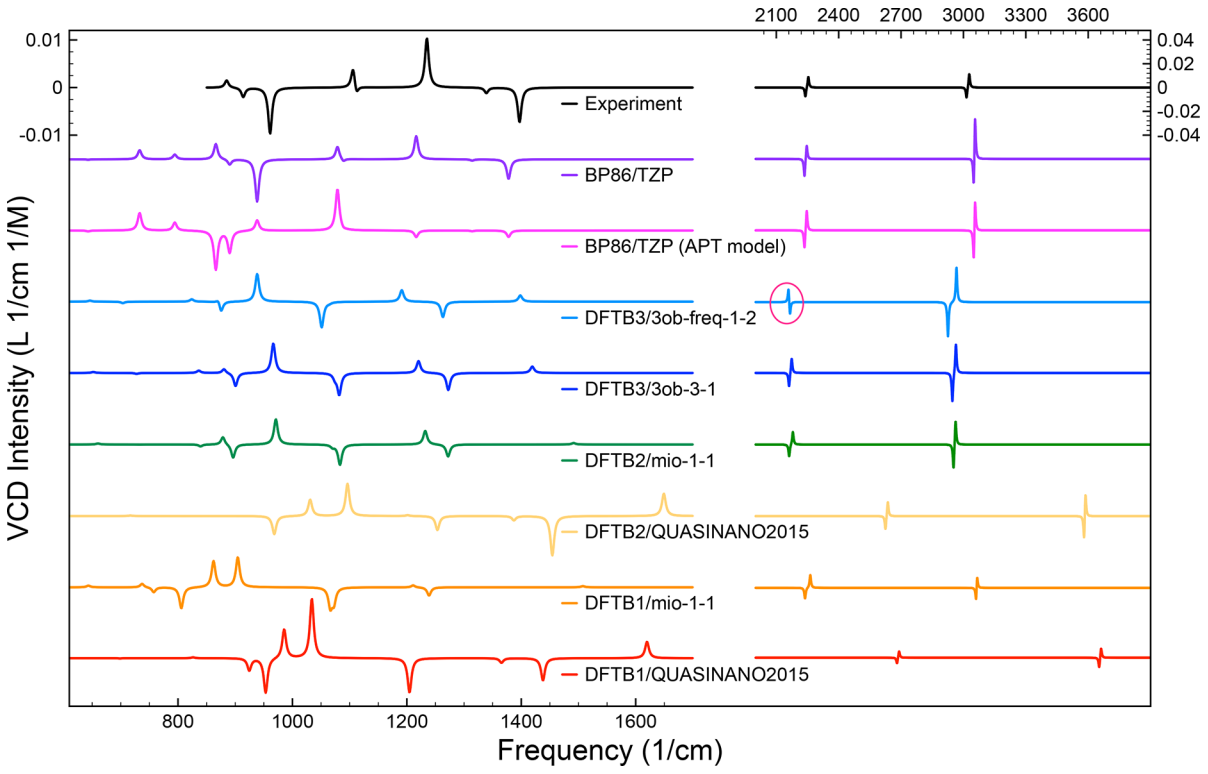

Figure 3. Comparison of VCD spectra of (*S*,*S*)-[2,3-$^2H_2$]oxirane (gas phase) calculated at several levels, and experimental data from ref 41. DFTB1/QUASINANO2015 intensities were rescaled by a factor of 0.25 for better visualization. Bands above 2000 cm^{-1} are displayed on a different scale (shown to the right and on the top) than those in the fingerprint region. Frequencies and rotational strengths are given in Table S1.

Table 1. Scalar Product (Overlap) between the (Mass-Weighted) Normal Modes Computed for (*S*,*S*)-[2,3-$^2H_2$]Oxirane (Gas Phase) at the Levels Shown in the Header[a] and Those at the BP86/TZP Level (the Reference)[b]

BP86/TZP		DFTB		DFTB2		DFTB3			
n^c	ν_n	qnano15	mio11	qnano15	mio11	3ob31	3obf12	BP86/SZ	avg[d]
1	643	0.99	1.00	0.99	1.00	1.00	1.00	1.00	1.00
2	733	1.00	0.96	0.99	0.99	0.99	0.98	1.00	0.99
3	794	0.90	0.99	$0.93^{(5)}$	0.97	0.99	0.99	$0.89^{(5)}$	0.95
4	866	0.96	0.79	0.86	$0.92^{(5)}$	$0.91^{(5)}$	$0.89^{(5)}$	0.94	0.92
5	890	0.90	0.99	$0.92^{(3)}$	$0.96^{(4)}$	$0.95^{(4)}$	$0.96^{(4)}$	$0.90^{(3)}$	0.92
6	938	0.96	0.83	0.72	0.91	0.89	0.86	0.91	0.87
7	1079	$1.00^{(8)}$	1.00	0.99	0.99	0.86	$0.97^{(8)}$	0.98	0.96
8	1089	$0.99^{(7)}$	0.94	0.79	0.98	0.86	$0.94^{(7)}$	0.94	0.93
9	1216	0.93	0.83	0.84	0.87	0.91	0.92	0.99	0.90
10	1314	1.00	1.00	1.00	1.00	0.99	1.00	1.00	1.00
11	1378	0.93	0.83	0.87	0.86	0.92	0.93	1.00	0.90
12	2236	1.00	1.00	1.00	1.00	0.96	$1.00^{(13)}$	1.00	0.99
13	2246	1.00	0.99	1.00	1.00	0.96	$1.00^{(12)}$	1.00	0.99
14	3050	1.00	1.00	$1.00^{(15)}$	1.00	0.94	1.00	1.00	0.99
15	3056	1.00	1.00	$1.00^{(14)}$	1.00	0.94	1.00	1.00	0.99

[a]Nomenclature of DFTB parametrizations is abbreviated. [b]Integers between parentheses next to the overlaps indicate with which *n*th BP86/TZP mode occurs the largest overlap. If nothing is specified, matching modes relate to the same *n* figure. [c]*n* refers to the energy order of the reference modes. [d]Averages are calculated after reordering of the modes according to the BP86/TZP order.

also be equal. Indeed, as observed in Table S2, DFTB modes with an overlap ≥0.99 (shown in bold) result in dipole strengths and rotational strengths that are less than, respectively, 10^{-39} and 1.7×10^{-44} esu^2 cm^2 different from the corresponding values from the BP86/TZP calculation. But even in the remaining cases, the relative magnitudes (and signs) of the majority of dipole and rotational strengths are well represented at any SCC-DFTB variant, with the only consistent error being the wrong sign of the rotational strength of mode 8 (overall a mode with one of the smallest overlaps). The difference is also clear when observing the significant reduction in the mean absolute error (MAE) values in Table S2 with respect to those in Table S1. Thus, the normal modes predicted by several of the DFTB variants seem sufficient to yield proper VA and VCD intensities, as long as higher level atomic tensors are applied, which is in agreement with the

DOI: 10.1021/acs.jpca.8b08218
J. Phys. Chem. A 2018, 122, 9435−9445

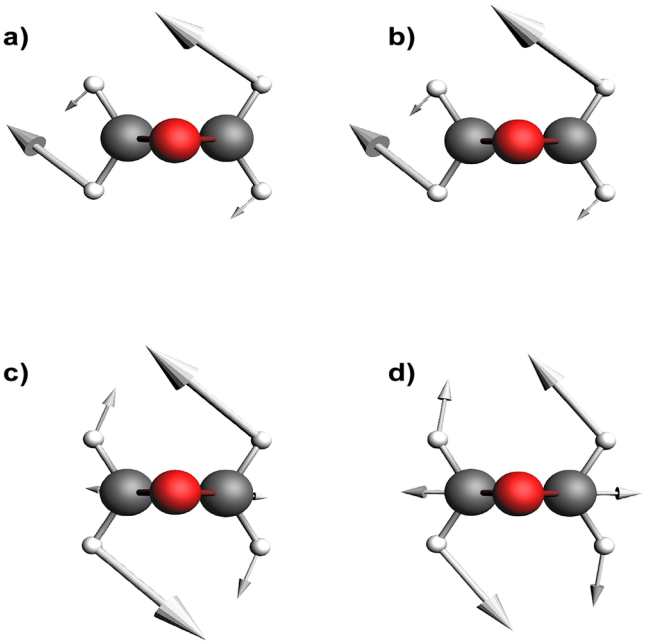

Figure 4. Representation of vibrational modes n = 10 (a and b) and n = 11 (c and d) calculated at BP86/TZP (left) and DFTB3/3ob-freq-1-2 (right) levels as viewed along the C−O−C plane.

conclusions in refs 21 and 22. The exception is DFTB1/mio-1-1, which still yields significant differences in the magnitudes (resulting in the largest MAEs).

Vibrational Frequencies. The second variable analyzed regards the vibrational frequencies (which are proportional to the eigenvalues of the mass-weighted Hessian). Although the DFTB dipole and rotational strengths shown in Table S2 are generally consistent with the BP86/TZP results, the modes were reordered in accordance with the overlaps shown in Table 1. The spectra of the fingerprint region calculated without such reordering are shown in Figures 5 and 6. The "composite" DFTB spectra displayed in these figures seem in fact considerably better than those from the "full" DFTB calculations in Figures 2 and 3, particularly the spectra obtained with the SCC-DFTB models and mio-1-1 or 3ob parameters. But a few differences with respect to the BP86/TZP spectra are noticeable. This is exemplified by the two bands in the frequency interval from ∼870 to ∼900 cm^{-1}, which are highlighted by the red rectangle in both Figures 5 and 6. As it was shown in Table 1, the main issue with these bands (modes 4 and 5) is actually the inversion in the order of their energies with respect to the BP86/TZP representation. Such inversions also explain the apparent failure of the DFTB3/3ob-freq-1-2 parametrization in correctly representing the signs of peaks 12 and 13 (highlighted by the red circle around 2200 cm^{-1} in the pertaining spectrum in Figure 3) while other DFTB variants had shown a proper agreement with BP86/TZP in the same region. Likewise, modes 7 and 8 in the BP86/TZP representation, which are separated in frequency by only 10 cm^{-1} (∼6 cm^{-1} experimentally), are inverted when calculated at some DFTB levels (DFTB1/QUASINANO2015 and DFTB3/3ob-freq-1-2). Summarizing, this basically means that, while the DFTB parametrizations may yield proper nuclear displacement vectors for some modes, not all these methods predict the same ordering for the normal-mode frequencies, which makes the comparison with experiment very difficult.

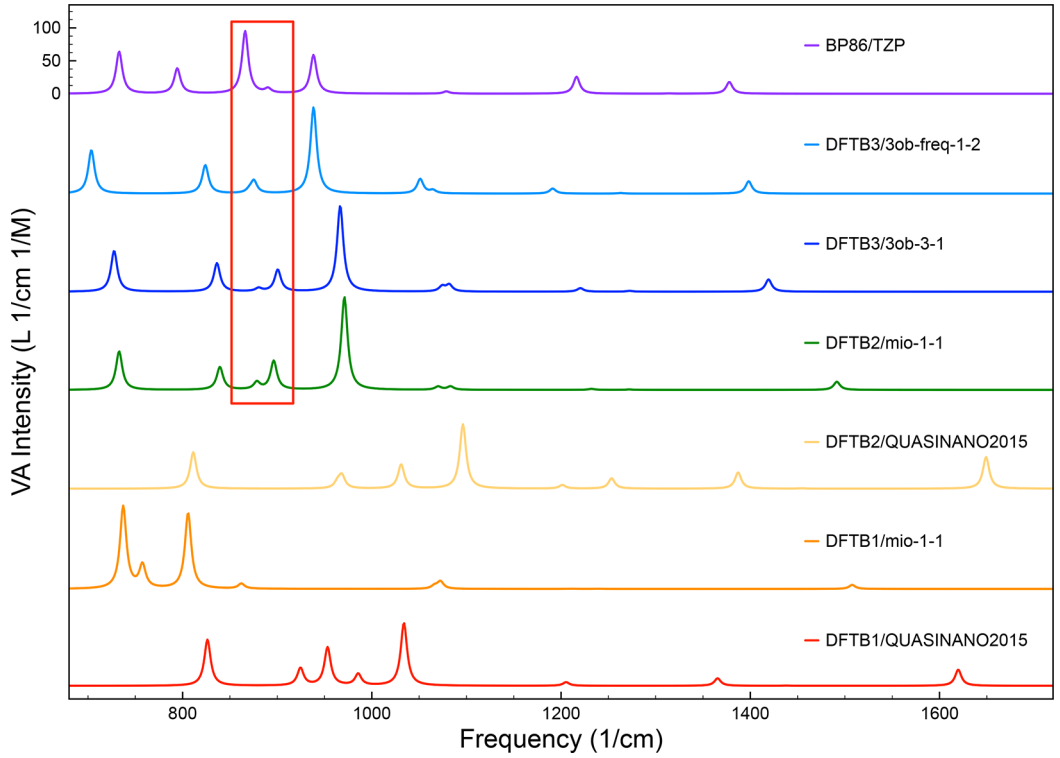

Figure 5. Comparison of VA spectra of (*S*,*S*)-[2,3-$^2H_2$]oxirane (gas phase) calculated at several levels. The DFTB spectra were obtained in a composite method in which the Hessian was calculated at each indicated level and the APTs/AATs were calculated at the BP86/TZP level. The red rectangle highlights an inversion in the order of the bands with respect to the BP86/TZP representation due to deviations in the DFTB frequencies.

DOI: 10.1021/acs.jpca.8b08218
J. Phys. Chem. A 2018, 122, 9435−9445

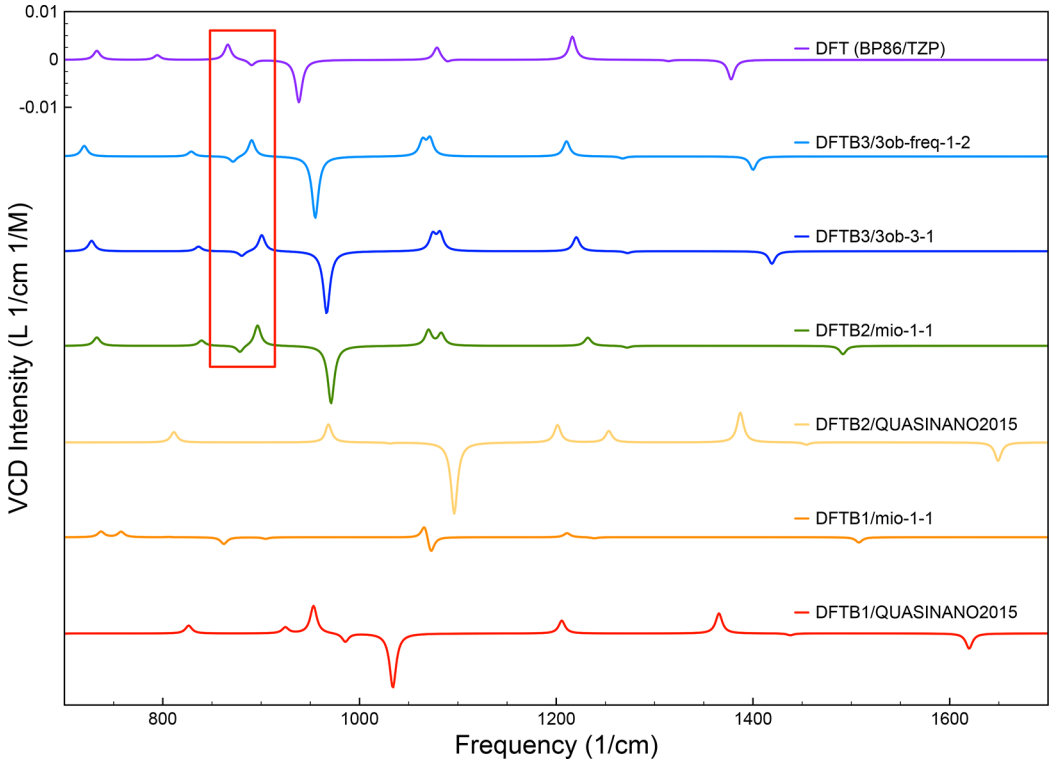

Figure 6. Comparison of VCD spectra of (*S*,*S*)-[2,3-$^2H_2$]oxirane (gas phase) calculated at several levels. The DFTB spectra were obtained in a composite method in which the Hessian was calculated at each indicated level and the APTs/AATs were calculated at the BP86/TZP level. The red rectangle highlights an inversion in the order of the bands with respect to the BP86/TZP representation due to deviations in the DFTB frequencies.

Another issue with the DFTB frequencies is the apparent random deviations with respect to the BP86/TZP results. By taking the DFTB3/3ob-freq-1-2 frequencies as an example, and reordering them according to the overlaps in Table 1, one finds deviations in the fingerprint region ranging from −76 to +7 cm^{-1}. In some cases, these deviations are also very significant, as it is the case with calculations with the QUASINANO2015 parameters, which yield frequencies up to 600 cm^{-1} higher than the BP86/TZP ones.

Electric Dipole Gradients. The final variable to be analyzed concerns the electric dipole gradient vectors. As in the model applied here for obtaining DFTB VCD intensities the magnetic tensor is approximated as a function of the APTs (eq 13), we proceed with this discussion by focusing on the dipole strengths, which are not affected by the same approximation. As already discussed in the analysis of the normal modes, the dipole gradients calculated with these standard DFTB methods are not adequate to be used in VA and VCD analyses (at least for oxirane). Symptomatic examples are the results obtained for mode 10. As shown in Table 1, this mode as calculated with the several DFTB variants is virtually identical to the equivalent BP86/TZP normal mode (overlaps ≥0.99 in all cases and no inversion of the energy order with other modes). However, while BP86/TZP calculates a near-zero dipole strength for this mode, most DFTB calculations yield one of the largest dipole strengths in the fingerprint region. Thus, the discrepancy must originate from inaccuracies in the electric dipole gradients.

Table S3 displays the norm of the dipole gradient vector upon displacing each atom in the *x*, *y*, and *z* directions, and the norm of the dipole moment vector at equilibrium. As one can notice, most DFTB variants predict dipole moments varying considerably from the BP86/TZP value. DFTB1 calculations yield dipole moments that are about (1.36 au with QUASINANO2015) or more (1.93 au with mio-1-1) than twice the BP86/TZP result (0.76 au). The SCC-DFTB models yield dipoles somewhat closer to the reference but still varying significantly depending on the choice of parameters, from 0.94 au with DFTB3/3ob-freq-1-2 to 0.72 au with DFTB2/QUASINANO2015. With regard to the dipole gradients, DFTB results deviate from the BP86/TZP values in a random fashion depending on the specific atom that is displaced and the direction. To test whether these inaccurate electric dipoles and gradients are a consequence of the point charges model in eq 10, electric dipoles were also obtained by integrating over the deformation density calculated by the DFTB2/QUASINANO2015 method (which yields the closest dipole norm to the reference, 0.72 au). The electric dipole norm changes slightly (to 0.80 au), but as shown in Table S1, the changes in the dipole gradients still yield dipole strengths quite different than the BP86/TZP values.

Therefore, we have learned from the analysis on oxirane that the analyzed DFTB methods can provide a reliable assessment of the normal-mode vectors. However, the energies of these modes deviate randomly from the BP86/TZP results, which may be misleading in the comparison with experimental data. Additionally, the electric dipole moment gradients (which yield the VA and VCD intensities) calculated with these DFTB variants are inaccurate, which substantially compromises the quality of the spectra. In order to validate these preliminary conclusions, we extend the analysis for two more systems. For simplification, we proceed with only one DFTB method, DFTB3/3ob-freq-1-2.

DOI: 10.1021/acs.jpca.8b08218
J. Phys. Chem. A 2018, 122, 9435−9445

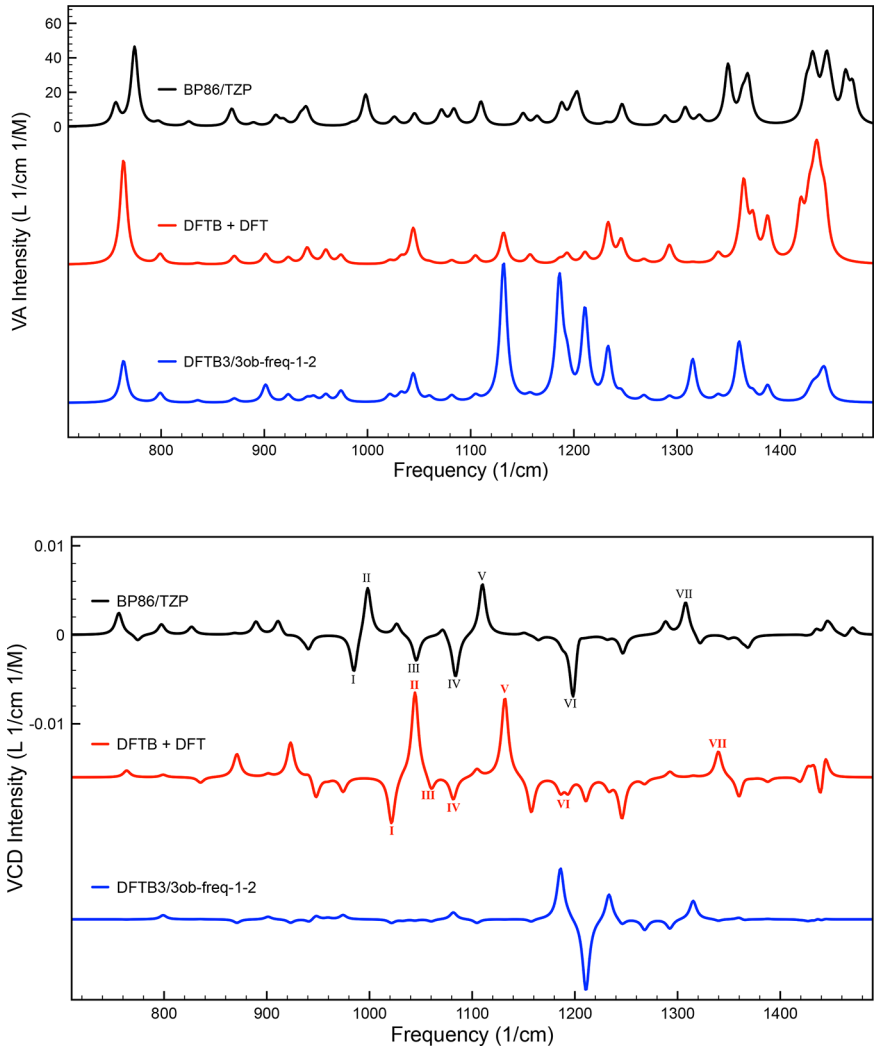

Figure 7. Comparison of VA (top) and VCD (bottom) spectra of (+)-α-pinene (gas phase) calculated at different levels. The spectra in red were obtained by combining the DFTB3/3ob-freq-1-2 Hessian with the BP86/TZP atomic polar and axial tensors (the latter only for VCD).

α-Pinene. The VA and VCD spectra of α-pinene from the BP86/TZP and DFTB3/3ob-freq-1-2 calculations, and from the composite method (DFTB3/3ob-freq-1-2 Hessian + BP86/TZP atomic axial and polar tensors), are shown in Figure 7. The differences in the VA and VCD spectra are again striking. The DFTB spectra differ significantly from the BP86/TZP ones, a level that is shown to nicely reproduce the VCD experiment.[27] As was the case for oxirane, a significant improvement on the DFTB spectra is obtained by combining the DFTB Hessian with APTs and AATs calculated at the BP86/TZP level. For example, the most intense peaks in the fingerprint region of the BP86/TZP VCD spectrum (indicated by Roman numerals) are well reproduced by the composite method as far as the signs are concerned, but larger differences still persist when the frequencies are considered.

The significance of the results discussed so far for this composite method is in the CPU time spent in the construction of the Hessian, which in general requires more than 90% of the computational time of a VCD calculation. The DFTB3/3ob-freq-1-2 computation of the Hessian takes less than a hundreth of the computational time spent on the BP86/TZP calculation. Additionally, as shown by Coriani et al.,[45] the AATs can be expressed as the frequency derivative at zero frequency of a linear response function within the density-matrix quasienergy formalism, which allows computing these magnetic tensors through only six response equations (three for the magnetic field responses and three for the frequency-perturbed density). As the APTs can also be calculated without using first-order perturbed densities with respect to nuclear displacements (as also shown in ref 45), it is possible to calculate these atomic tensors separately from the Hessian. This approach is already used in, e.g., the VCD implementation within the Dalton program suite.[46] Hence, on the basis of the results shown for oxirane and α-pinene, an implementation of Coriani's equations in a DFTB/DFT framework would allow for much faster, and yet accurate, calculations than currently possible. Such an implementation is currently also being realized in ADF.

Dydrogesterone. The comparison of VA and VCD spectra of dydrogesterone is plotted in Figure 8. The spectra calculated with the DFTB3/3ob-freq-1-2 method seem again to at most replicate some qualitative features of the BP86/TZP spectra, i.e., the presence of very intense peaks in the VA spectrum from ~1550 to ~1800 cm^{-1} related to C═O and C═C stretches, and the signs of some peaks in the VCD spectrum from ~1100 to ~1350 cm^{-1}. But unlike in the previous cases, little improvement is attained with replacing the APTs and AATs for the DFT ones. As we have already

DOI: 10.1021/acs.jpca.8b08218
J. Phys. Chem. A 2018, 122, 9435−9445

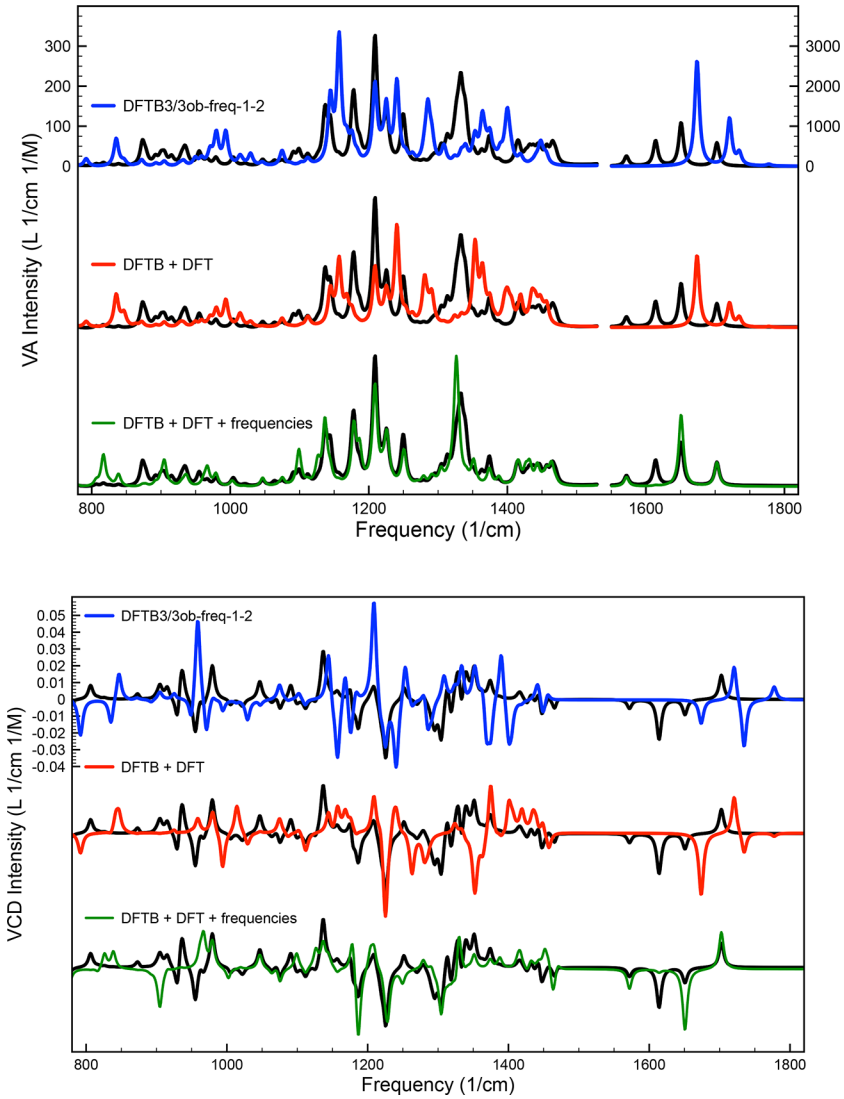

Figure 8. Comparison of VA (top) and VCD (bottom) spectra of dydrogesterone (gas phase) calculated at different levels. The black spectra were obtained at the BP86/TZP level. The spectra in red were calculated by combining the DFTB3/3ob-freq-1-2 Hessian with the BP86/TZP atomic polar and axial tensors. The spectra in green were obtained by additionally positioning the DFTB3/3ob-freq-1-2 bands according to the frequencies calculated at the BP86/TZP level (and reordering them according to an overlap analysis similar to that shown in Table 1). The VCD intensities calculated at the DFTB3/3ob-freq-1-2 level (blue spectrum) were rescaled by a factor of 4.0 for better visualization. VA bands above 1550 cm^{-1} are displayed on a different scale (shown to the right) than those in the fingerprint region.

discussed, the DFTB frequencies deviate in a nonlinear fashion from the DFT reference. With the fingerprint region of dydrogesterone containing more normal modes than in the case of the smaller molecules, these deviations start playing a bigger role in the representation of the spectra. This is easy to visualize in a simple thought experiment. If two peaks of a VCD spectrum with opposite signs and similar magnitudes become near-degenerate due to these deviations, they will cancel each other out, completely changing the shape of the spectrum in that region. The green spectra in Figure 8 are the result from replacing the DFTB frequencies in the composite method for the DFT ones. These frequencies are also reordered in accordance with the overlap results; i.e., the DFTB modes are placed in the position of the BP86/TZP modes with which the highest overlap is attained. The match with the full DFT calculation considerably improves.

Therefore, even though the combination of a DFTB Hessian with DFT atomic polar and axial tensors has been shown to be an interesting tool for speeding up VA and VCD calculations, the random deviations in the DFTB frequencies are likely to be the limiting factor of such a composite method for comparing the spectra of large molecules with the experiment. Alternatives for obtaining better frequencies include the use of scaling methods[47] and partial Hessian techniques,[48−51] which could be applied in combination with Coriani's[45] equations.

CONCLUSIONS

We have analyzed the performance of DFTB for obtaining VCD spectra through an approximate model. The overall performance of standard DFTB parametrizations was rather poor, particularly the calculations without self-consistency cycles (DFTB1) and/or with QUASINANO2015 parameters. A decomposition analysis showed that (1) the normal modes calculated with several DFTB variants reasonably replicate the respective BP86/TZP vectors, but (2) the random deviations observed in the vibrational frequencies of such modes yield

DOI: 10.1021/acs.jpca.8b08218
J. Phys. Chem. A 2018, 122, 9435−9445

bands that are difficult to match with the experiment, and, additionally, (3) the electric dipole gradients are in general inaccurate, rendering bad VA and VCD intensities.

The latter issue can be fixed by separating these vibrational calculations in two stages where the least demanding step, obtaining the atomic polar and axial tensors,[45] is realized at a higher level of theory (as DFT). As the deviations in the frequencies can also be tackled,[47−51] DFTB can be a quicker route for obtaining accurate vibrational spectra if applied in these composite schemes.

It should be emphasized that calculations at a full DFTB level could still be applied in VCD evaluations if new parametrizations improve the description of electric dipole moments and/or vibrational frequencies. Thus, the DFTB-VCD code used throughout this study was added in the latest development version of the ADF modeling suite (without the 1/4 factor in eq 12 to ajdust for the usually low VCD intensities obtained with SCC-DFTB methods), and is available in the 2018 release version of the package. Spectra decomposition tools are also available.[44,52] A tutorial on how to perform these calculations and using such tools is available on the website https://www.scm.com.

■ ASSOCIATED CONTENT

Supporting Information

The Supporting Information is available free of charge on the ACS Publications website at DOI: 10.1021/acs.jpca.8b08218.

(*S*,*S*)-[2,3-$^2H_2$]oxirane harmonic vibrational frequencies, dipole strengths, rotational strengths; norms of electric dipole moments and electric dipole moment derivatives (PDF)

■ AUTHOR INFORMATION

Corresponding Author

*E-mail: l.visscher@vu.nl.

ORCID

T. Q. Teodoro: 0000-0003-4590-0056

S. E. Galembeck: 0000-0001-5018-4643

L. Visscher: 0000-0002-7748-6243

Notes

The authors declare no competing financial interest.

■ ACKNOWLEDGMENTS

This research received funding from The Netherlands Organisation for Scientific Research in the framework of the Fund New Chemical Innovations (NWO Project No. 731.014.209). T.Q.T. thanks the São Paulo Research Foundation (FAPESP Project Nos. 2016/07787-4 and 2016/23165-3) for a postdoctoral grant. S.E.G. also acknowledges FAPESP (Project Nos. 2008/02677-0 and 2014/50265-3) and the National Council for Scientific and Technological Development (CNPq Project No. 308254/2016-3). We also thank Dr. Stan van Gisbergen for useful discussions and the SCM team for technical support.

■ REFERENCES

(1) Hsu, E. C.; Holzwarth, G. Vibrational circular dichroism observed in crystalline α-$NiSO_4{\cdot}6H_2O$ and α-$ZnSeO_4{\cdot}6H_2O$ between 1900 and 5000 cm^{-1}. *J. Chem. Phys.* **1973**, *59*, 4678−4685.

(2) Holzwarth, G.; Hsu, E. C.; Mosher, H. S.; Faulkner, T. R.; Moscowitz, A. Infrared circular dichroism of carbon-hydrogen and carbon-deuterium stretching modes. Observations. *J. Am. Chem. Soc.* **1974**, *96*, 251−252.

(3) Barron, L. D.; Buckingham, A. D. Vibrational optical activity. *Chem. Phys. Lett.* **2010**, *492*, 199−213.

(4) Nafie, L. A. *Vibrational Optical Activity: Principles and Applications*; John Wiley & Sons: 2011.

(5) Polavarapu, P. L. *Chiroptical Spectroscopy: Fundamentals and Applications*; CRC Press: 2017.

(6) Berova, N.; Polavarapu, P. L.; Nakanishi, K.; Woody, R. W. *Comprehensive Chiroptical Spectrosocopy*; John Wiley & Sons: New York, NY, 2012; Vol. *1*.

(7) Berova, N.; Polavarapu, P. L.; Nakanishi, K.; Woody, R. W. *Comprehensive Chiroptical Spectrosocopy*; John Wiley & Sons: New York, NY, 2012; Vol. *2*.

(8) Stephens, P. J.; Devlin, F. J.; Cheeseman, J. R. *VCD Spectroscopy for Organic Chemists*; CRC Press: 2012.

(9) Stephens, P. J. Theory of vibrational circular dichroism. *J. Phys. Chem.* **1985**, *89*, 748−752.

(10) Heshmat, M.; Nicu, V. P.; Baerends, E. J. On the Equivalence of Conformational and Enantiomeric Changes of Atomic Configuration for Vibrational Circular Dichroism Signs. *J. Phys. Chem. A* **2012**, *116*, 3454−3464.

(11) Urbanová, M. Bioinspired interactions studied by vibrational circular dichroism. *Chirality* **2009**, *21*, E215−E230.

(12) Seifert, G.; Porezag, D.; Frauenheim, T. Calculations of molecules, clusters, and solids with a simplified LCAO-DFT-LDA scheme. *Int. J. Quantum Chem.* **1996**, *58*, 185−192.

(13) Porezag, D.; Frauenheim, T.; Köhler, T.; Seifert, G.; Kaschner, R. Construction of tight-binding-like potentials on the basis of density-functional theory: Application to carbon. *Phys. Rev. B: Condens. Matter Mater. Phys.* **1995**, *51*, 12947.

(14) Elstner, M.; Jalkanen, K.; Knapp-Mohammady, M.; Frauenheim, T.; Suhai, S. DFT studies on helix formation in N-acetyl-(L-alanyl) n-N-methylamide for n= 1−20. *Chem. Phys.* **2000**, *256*, 15−27.

(15) Abdali, S.; Niehaus, T. A.; Jalkanen, K. J.; Cao, X.; Nafie, L.; Frauenheim, T.; Suhai, S.; Bohr, H. Vibrational absorption spectra, DFT and SCC-DFTB conformational study and analysis of [Leu] enkephalin. *Phys. Chem. Chem. Phys.* **2003**, *5*, 1295−1300.

(16) Zheng, G.; Irle, S.; Morokuma, K. Performance of the DFTB method in comparison to DFT and semiempirical methods for geometries and energies of C 20−C 86 fullerene isomers. *Chem. Phys. Lett.* **2005**, *412*, 210−216.

(17) Elstner, M. The SCC-DFTB method and its application to biological systems. *Theor. Chem. Acc.* **2006**, *116*, 316−325.

(18) Brandenburg, J. G.; Grimme, S. Accurate modeling of organic molecular crystals by dispersion-corrected density functional tight binding (DFTB). *J. Phys. Chem. Lett.* **2014**, *5*, 1785−1789.

(19) Nénon, S.; Champagne, B. SCC-DFTB calculation of the static first hyperpolarizability: From gas phase molecules to functionalized surfaces. *J. Chem. Phys.* **2013**, *138*, 204107.

(20) de Wergifosse, M.; Grimme, S. Nonlinear-response properties in a simplified time-dependent density functional theory (sTD-DFT) framework: Evaluation of the first hyperpolarizability. *J. Chem. Phys.* **2018**, *149*, 024108.

(21) Bohr, H.; Jalkanen, K. J.; Elstner, M.; Frimand, K.; Suhai, S. A comparative study of MP2, B3LYP, RHF and SCC-DFTB force fields in predicting the vibrational spectra of N-acetyl-L-alanine-N′-methyl amide: VA and VCD spectra. *Chem. Phys.* **1999**, *246*, 13−36.

(22) Frimand, K.; Jalkanen, K. J. SCC-TB, DFT/B3LYP, MP2, AM1, PM3 and RHF study of ethylene oxide and propylene oxide structures, VA and VCD spectra. *Chem. Phys.* **2002**, *279*, 161−178.

(23) Rüger, R.; Yakovlev, A.; Philipsen, P.; Borini, S.; Melix, P.; Oliveira, A. F.; Franchini, M.; Soini, T.; de Reus, M.; Ghorbani Asl, M.; et al. *ADF DFTB 2017*; SCM, Theoretical Chemistry, Vrije Universiteit: Amsterdam, The Netherlands. https://www.scm.com (accessed Nov 9, 2018).

(24) Baerends, E. J.; Ziegler, T.; Atkins, A. J.; Autschbach, J.; Bashford, D.; Baseggio, O.; Bérces, A.; Bickelhaupt, F. M.; Bo, C.;

DOI: 10.1021/acs.jpca.8b08218
J. Phys. Chem. A 2018, 122, 9435−9445

Boerritger, P. M.; et al. *ADF 2017*; SCM, Theoretical Chemistry, Vrije Universiteit: Amsterdam, The Netherlands. https://www.scm.com (accessed Nov 9, 2018).
(25) te Velde, G.; Bickelhaupt, F. M.; Baerends, E. J.; Fonseca Guerra, C.; van Gisbergen, S. J. A.; Snijders, J. G.; Ziegler, T. Chemistry with ADF. *J. Comput. Chem.* **2001**, *22*, 931−967.
(26) Person, W. B.; Newton, J. H. Dipole moment derivatives and infrared intensities. I. Polar tensors. *J. Chem. Phys.* **1974**, *61*, 1040−1049.
(27) Nicu, V. P.; Neugebauer, J.; Wolff, S. K.; Baerends, E. J. A vibrational circular dichroism implementation within a Slater-type-orbital based density functional framework and its application to hexa- and hepta-helicenes. *Theor. Chem. Acc.* **2008**, *119*, 245−263.
(28) Oliveira, A. F.; Seifert, G.; Heine, T.; Duarte, H. A. Density-functional based tight-binding: an approximate DFT method. *J. Braz. Chem. Soc.* **2009**, *20*, 1193−1205.
(29) Slater, J. C.; Koster, G. F. Simplified LCAO method for the periodic potential problem. *Phys. Rev.* **1954**, *94*, 1498.
(30) Elstner, M.; Porezag, D.; Jungnickel, G.; Elsner, J.; Haugk, M.; Frauenheim, T.; Suhai, S.; Seifert, G. Self-consistent-charge density-functional tight-binding method for simulations of complex materials properties. *Phys. Rev. B: Condens. Matter Mater. Phys.* **1998**, *58*, 7260−7268.
(31) Gaus, M.; Cui, Q.; Elstner, M. DFTB3: Extension of the Self-Consistent-Charge Density-Functional Tight-Binding Method (SCC-DFTB). *J. Chem. Theory Comput.* **2011**, *7*, 931−948.
(32) Mulliken, R. S. Electronic Population Analysis on LCAO-MO Molecular Wave Functions. I. *J. Chem. Phys.* **1955**, *23*, 1833−1840.
(33) Freedman, T. B.; Nafie, L. A. Vibrational optical activity calculations using infrared and Raman atomic polar tensors. *J. Chem. Phys.* **1983**, *78*, 27−31.
(34) Stephens, P. J. Gauge dependence of vibrational magnetic dipole transition moments and rotational strengths. *J. Phys. Chem.* **1987**, *91*, 1712−1715.
(35) Becke, A. D. Density-functional exchange-energy approximation with correct asymptotic behavior. *Phys. Rev. A: At., Mol., Opt. Phys.* **1988**, *38*, 3098−3100.
(36) Perdew, J. P. Density-functional approximation for the correlation energy of the inhomogeneous electron gas. *Phys. Rev. B: Condens. Matter Mater. Phys.* **1986**, *33*, 8822−8824.
(37) Perdew, J. P. Erratum: Density-functional approximation for the correlation energy of the inhomogeneous electron gas. *Phys. Rev. B: Condens. Matter Mater. Phys.* **1986**, *34*, 7406−7406.
(38) Van Lenthe, E.; Baerends, E. J. Optimized Slater-type basis sets for the elements 1−118. *J. Comput. Chem.* **2003**, *24*, 1142−1156.
(39) Gaus, M.; Goez, A.; Elstner, M. Parametrization and Benchmark of DFTB3 for Organic Molecules. *J. Chem. Theory Comput.* **2013**, *9*, 338−354.
(40) Oliveira, A. F.; Philipsen, P.; Heine, T. DFTB Parameters for the Periodic Table, Part 2: Energies and Energy Gradients from Hydrogen to Calcium. *J. Chem. Theory Comput.* **2015**, *11*, 5209−5218.
(41) Freedman, T. B.; Spencer, K. M.; Ragunathan, N.; Nafie, L. A.; Moore, J. A.; Schwab, J. M. Vibrational circular dichroism of (S,S)-[2,3−2H2]oxirane in the gas phase and in solution. *Can. J. Chem.* **1991**, *69*, 1619−1629.
(42) Dutler, R.; Rauk, A. Calculated infrared absorption and vibrational circular dichroism intensities of oxirane and its deuterated analogs. *J. Am. Chem. Soc.* **1989**, *111*, 6957−6966.
(43) Kawiecki, R.; Devlin, F.; Stephens, P.; Amos, R. Vibrational circular dichroism of propylene oxide. *J. Phys. Chem.* **1991**, *95*, 9817−9831.
(44) Nicu, V. P. Revisiting an old concept: the coupled oscillator model for VCD. Part 2: implications of the generalised coupled oscillator mechanism for the VCD robustness concept. *Phys. Chem. Chem. Phys.* **2016**, *18*, 21213−21225.
(45) Coriani, S.; Thorvaldsen, A. J.; Kristensen, K.; Jorgensen, P. Variational response-function formulation of vibrational circular dichroism. *Phys. Chem. Chem. Phys.* **2011**, *13*, 4224−4229.
(46) Aidas, K.; Angeli, C.; Bak, K. L.; Bakken, V.; Bast, R.; Boman, L.; Christiansen, O.; Cimiraglia, R.; Coriani, S.; Dahle, P.; et al. The Dalton quantum chemistry program system. *WIREs Comput. Mol. Sci.* **2014**, *4*, 269−284.
(47) Baker, J.; Jarzecki, A. A.; Pulay, P. Direct Scaling of Primitive Valence Force Constants: An Alternative Approach to Scaled Quantum Mechanical Force Fields. *J. Phys. Chem. A* **1998**, *102*, 1412−1424.
(48) Li, H.; Jensen, J. H. Partial Hessian vibrational analysis: the localization of the molecular vibrational energy and entropy. *Theor. Chem. Acc.* **2002**, *107*, 211−219.
(49) Ghysels, A.; Van Neck, D.; Van Speybroeck, V.; Verstraelen, T.; Waroquier, M. Vibrational modes in partially optimized molecular systems. *J. Chem. Phys.* **2007**, *126*, 224102.
(50) Jacob, C. R.; Reiher, M. Localizing normal modes in large molecules. *J. Chem. Phys.* **2009**, *130*, 084106.
(51) Woodcock, H. L.; Zheng, W.; Ghysels, A.; Shao, Y.; Kong, J.; Brooks, B. R. Vibrational subsystem analysis: A method for probing free energies and correlations in the harmonic limit. *J. Chem. Phys.* **2008**, *129*, 214109.
(52) Nicu, V. P. Revisiting an old concept: the coupled oscillator model for VCD. Part 1: the generalised coupled oscillator mechanism and its intrinsic connection to the strength of VCD signals. *Phys. Chem. Chem. Phys.* **2016**, *18*, 21202−21212.

DOI: 10.1021/acs.jpca.8b08218
J. Phys. Chem. A 2018, 122, 9435−9445